ISSN 0001-4370, Oceanology, 2016, Vol. 56, No. 4, pp. 470–482. © Pleiades Publishing, Inc., 2016.
Original Russian Text © P.N. Golovin, N.N. Antipov, A.V. Klepikov, 2016, published in Okeanologiya, 2016, Vol. 56, No. 4, pp. 514–528.

MARINE PHYSICS

Intrusive Layering of the Antarctic Slope Front

P. N. Golovin, N. N. Antipov, and A. V. Klepikov

Arctic and Antarctic Research Institute, ul. Beringa 38, St. Petersburg, 199397 Russia
e-mail: golovin@aari.ru

Received May 21, 2014; in final form, November 19, 2014

Abstract—Cascading of cold Antarctic shelf water (ASW) initiates compensatory isopycnic upwelling of the warm Circumpolar Deep Water (CDW). The baroclinic/thermoclinic Antarctic slope front (ASF) is formed, and a mesoscale intrusive structure develops on the shelf edge and slope. Mesoscale processes when the ASF peaks are periodically accompanied by local baroclinic instability, which forms a smaller-scale intrusive structure. Therefore, the ASF is naturally subdivided into two layers according to the intrusion scales (vertical δH and horizontal L) and the horizontal parameters of the front (thermoclinity $(T_L)_\rho$ and baroclinity γ_ρ). Analysis of ASF intrusive layering due to the baroclinic factor supports the following conclusion: the higher the $(T_L)_\rho$ of the ASF, the greater the intrusion intensity $|\delta\theta|$ (temperature anomaly amplitude), while an increase in γ_ρ of the ASF leads to a decrease in intrusion scales δH and L. Frontal intrusions can be distinguished by a development degree. Regardless of the degree of development, all warm intrusions are characterized by vertical density stratification, while cold intrusions are characterized by density quasihomogeneity. According to field data, the ASF instability process is subdivided into four stages. When theASF is baroclinically unstable, the local baroclinic deformation radius Rd_L of the front is close in magnitude to the horizontal scale L of the intrusions that form, and their characteristic vertical scale δH is close to the typical vertical scale of front instability.

DOI: 10.1134/S0001437016030085

INTRODUCTION

The potential temperature θ and salinity S profiles most often demonstrate well-defined finely structured fluctuations controlling the intense process of intrusive layering in oceanic frontal zones, where water interacts with different thermohaline characteristics [15]. Intrusions develop in thermohaline fronts due to different generation mechanisms and structure-forming processes [10]. The generation mechanisms include various front instabilities responsible for intrusive layering, which form vertical quasiperiodic or regular intrusive structures. The basic generation mechanisms include thermohaline instability or instability related to double diffusion processes; baroclinic instability; and shear instability, in particular, the Kelvin–Helmholtz instability. Structure-forming processes such as vertical mixing and lateral advection generate thicker, but single vertical intrusions [10].

According to aforesaid, there is no consistent pattern in the increase in the intrusion layering intensity in the field of various oceanic fronts depending on such mesoscale horizontal parameters as the degree of baroclinity and thermoclinity [10, 17]. For example, in the Kuroshio front zone [16], an increase in the degree of baroclinity reduces the vertical scale of frontal intrusions, while an increase in the degree of thermoclinity leads to an increase in absolute temperature anomalies in these intrusions. An increase in the degree of baroclinity in the frontal region of the Gulf Stream prevents intrusion layering processes related to double diffusion, while the front thermoclinity is high in this case [8]. According to data on the subarctic frontal zone of the Pacific Ocean [11], a higher front baroclinity can prevent the formation of intrusions related to thermohaline instability, but can increase the role of baroclinic instability in the intrusion generation processes [12]. In the South Polar Frontal Zone (SPFZ), which is characterized by a high baroclinity, baroclinic instability plays a major role in intrusion laying [6], and the front is assumed to be packed by submesoscale vortex intrusions interacting with each other with equal density. A parallel study [17] confirms that an increase in the SPFZ baroclinity decreases the intensity of isopycnic processes, but intensifies diapycnic processes accompanying baroclinic instability enabled by insignificant stratification of Antarctic waters.

The shelf and slope water interaction areas at the shelf edges where slope fronts are formed [15] are peculiar in the World Ocean. The main difference from open ocean fronts is the influence of the bottom topography (a dramatic increase in the bottom slope within the shelf edge) on the formation of slope edges, their future dynamics, instability, and intrusive layering in the front area [3, 4].

This paper considers the formation conditions of the Antarctic slope front (ASF) in the Cooperation

Sea. The ASF local thermohaline and density structure reflecting the ASF dynamics is analyzed. Intrusive layering of the ASF is studied in detail, and the considered intrusions are classified. We attempt to determine the main generation mechanism responsible for intrusive layering and to identify the relationships between characteristics of the front intrusions and horizontal parameters of the front. The study is based on the field data of targeted hydrological observations made with a low spatial interval in profiles across the shelf and continental slope in the Cooperation Sea and Prydz Bay in the Antarctic region in 2004–2007 and 2011–2013 [1, 2, 4]. Figure 1a shows the field observation scheme. It also includes observations for 2015. Thermohaline measurements were carried out with a standard probe, such as Sea Bird SBE 911 plus CTD.

ASF FORMATION AND DYNAMIC CHARACTERISTICS

ASF formation at the shelf edge and top of the slope in the Cooperation Sea occurs due to the flow of Antarctic shelf water (ASW). Within the ASF, cold and less saline (denser) ASW interacts with warm and more saline (less dense) Circumpolar Deep Water (CDW) (the temperature difference reaches 1.2–2.2°C). Shelf and slope cascading (in deep parts of the continental slope) is also observed in summer, when there is no convection for ASW generation in areas with uncovered near-barrier and flaw polynya in winter [4]. In summer, the dense water flow in the slope is fed by huge ASW volumes that accumulate in winter in relatively deep-water shelf depressions [4, 18]. In other words, cascading is one of the major processes initiating the intense circulation at the shelf edge and continental slope [3, 4]. Nevertheless, it should be noted that the CDW transformation efficiency in the ASF area and, as a consequence, local structure of the front are also related to the spatial and temporal variability of the CDW distribution [4].

The gravitational flow of ASWs quasihomogeneous in density, temperature, and salinity is quasi-isopycnic (Figs. 1b, 1c). However, when spreading over a sloped bottom, cold and dense ASW flows interacting with CDW form baroclinic–thermoclinic front water interface, the ASF. Due to continuous movement in the near-slope area, the cascading is accompanied by compensatory intrusive CDW upwelling along the inclined ASF isopycnals (Fig. 1b). According to the observation data, warm CDW intrusions are characterized by a vertical density stratification, but they extend in a quasi-isopycnic manner (Fig. 1c).

Thus, ASW cascading and CDW upwelling are mesoscale structure-forming processes generating an intrusion structure on the shelf edge and offshore. In this case, compensatory upwelling is an analog of horizontal advection. Then, CDW penetrates the shelf in a modified state (MCDW) as large warm intrusions or, occasionally, as vortex intrusions [4]. In the θ and S profiles, the thickness of these single intrusions reaches 100–250 m (Fig. 1c). The MCDW distribution in the shelf is observed, to a lesser or greater extent, in all profiles made in different parts of the Cooperation Sea [1, 2, 4].

ASW cascading is spatially discrete 3D movement of an eventful (pulsed) nature. It can be forced, as discrete meanderings still related to the ASW front; or free, as discrete plumes already detached from the front [3, 4]. Such an ASW flow pattern controls the nature of CDW compensatory upwelling. In certain periods, these processes appear geostrophically balanced: the spread of CDW intrusions seems dynamically stable (Fig. 1b). However, finely structured components demonstrating small-scale instability during CDW and ASW interaction are already noticeable in the thermohaline and dense profiles in the shelf (Fig. 1c).

Analysis of the profiles revealed many signs pointing to the 3D nature of the ASW flow on the shelf edge and at the top of the slope [4, 5]. This specific feature of cascading is likely able to affect the unstable nature of the baroclinic–thermoclinic ASF. It can be assumed that the 3D baroclinic instability is the main reason for the ASF instability and subsequent intrusive layering [5]. These conclusions were based on joint analysis of the generalized laboratory results obtained from studying the stability in bottom gravitational flows, baroclinic fronts, and vortex lenses [7], as well as from field observation data [4, 5]. The baroclinic instability likely develops on the background of mesoscale structure-forming processes of cascading and upwelling after the local ASF peaking and is less extensive. These assumptions will be confirmed by detailed study of the characteristic features of thermohaline intrusions in relation to the horizontal ASF parameters.

DETERMINATION OF ASF PARAMETERS AND FRONT INTRUSION CHARACTERISTICS

The intrusion layering characteristics were obtained by identification of a finely structured component on the potential temperature θ profiles by subtracting the linearly approximated temperature profile from the profile actually measured at stations of the front region (Fig. 2). Calculation of the intrusion layer thickness δH and temperature anomaly amplitude $\delta\theta$ in this layer (Fig. 2) corresponds to the method applied to the SPFZ [6]. An isopycnic surface consistent with the occurrence depth $\delta\theta$ is assumed to be an intrusion surface.

The ASF horizontal parameter, the degree of baroclinity, is determined as the slope of the isopycnals to isobars $\gamma_\rho = \Delta z/X$, where Δz is the maximum variation in depth of the intrusion isopycnic surface between adjacent stations in the transfrontal profile and X is distance between stations [6, 8, 11]. In addition, the front baroclinity is characterized by the Richardson

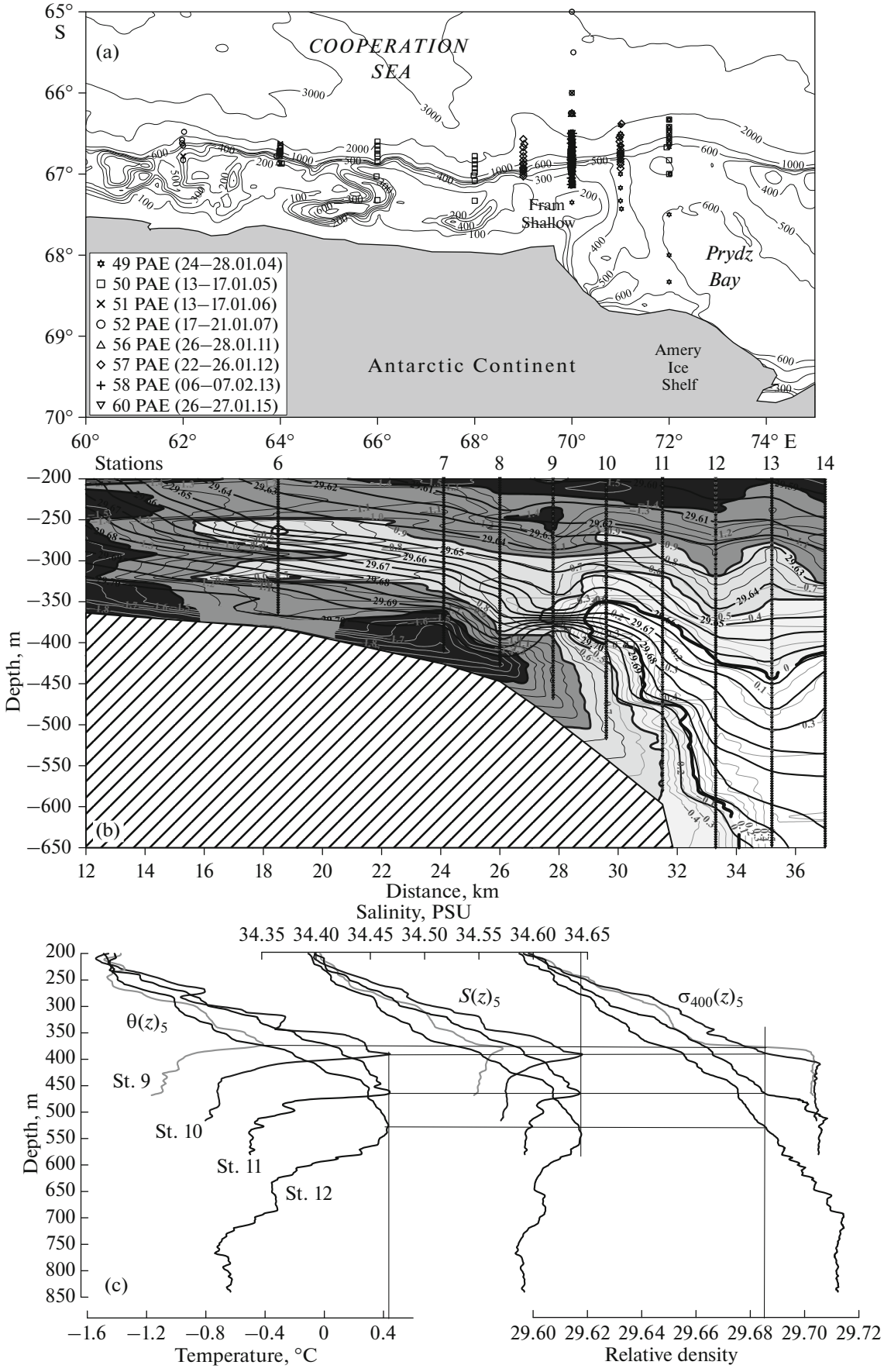
(a)
COOPERATION SEA
Fram Shallow
Prydz Bay
Antarctic Continent
Amery Ice Shelf
49 PAE (24–28.01.04)
50 PAE (13–17.01.05)
51 PAE (13–17.01.06)
52 PAE (17–21.01.07)
56 PAE (26–28.01.11)
57 PAE (22–26.01.12)
58 PAE (06–07.02.13)
60 PAE (26–27.01.15)
65° S
66°
67°
68°
69°
70°
60° 62° 64° 66° 68° 70° 72° 74° E
Stations 6 7 8 9 10 11 12 13 14
(b)
Depth, m
Distance, km
Salinity, PSU
34.35 34.40 34.45 34.50 34.55 34.60 34.65
$S(z)_5$
$\sigma_{400}(z)_5$
$\theta(z)_5$
St. 9
St. 10
St. 11
St. 12
(c)
Temperature, °C
Relative density
29.60 29.62 29.64 29.66 29.68 29.70 29.72

Fig. 1. (a) Hydrological observations by R/V *Akademik Fedorov* on shelf and continental slope in Cooperation Sea on seasonal expeditions of Russian Antarctic Expedition (RAE) in January and February 2004–2007, 2011–2013, and 2015 (thin lines indicate isobaths). (b) Joint profile of potential temperature θ°C (at $p = p_a$) and relative potential density σ_{400} (in relation to reference level of p = 400 db) directed across shelf and continental slope at 70° E and carried out in January 2013 in Cooperation Sea. (c) $\theta(z)$, $S(z)$, and $\sigma_{400}(z)$ profiles (smoothed by sliding average over five values, index 5) at the shelf edge and continental slope at stations 9, 10, 11, and 12, where profiles cross warm CDW intrusion, which rises and extends isopycnically over shelf.

number in the stratified geostrophic flow $\mathrm{Ri}_g = (f/N\gamma_\rho)^2$ [13] and baroclinity parameter $\varepsilon \equiv \mathrm{Ri}_g^{-1/2}$ [8, 11]. The Ri_g value also gives an idea of the local stability of the front. In this case, f is the Coriolis parameter, N is the Vaisala–Brent background frequency in the intrusion formation layer. In the Cooperation Sea and Prydz Bay, at the shelf edge, $N \approx (2–3) \times 10^{-3}$ s^{-1} and $f \approx 1.4 \times 10^{-4}$ s^{-1}. Another ASF horizontal parameter, the degree of thermoclinity, is characterized by the isopycnic temperature gradient $(T_L)_\rho = (\Delta\theta_{ip}/X)_\rho$, where $\Delta\theta_{ip}$ is the maximum variation in the potential temperature on the intrusion surface between adjacent stations in the transfrontal profile [6, 8, 11, 12].

The main mechanisms of intrusive layering of the baroclinic–thermoclinic fronts include thermohaline instability caused by double diffusion [10] and baroclinic instability [6, 8, 9, 11, 16]. The baroclinity value $\varepsilon \equiv \mathrm{Ri}_g^{-1/2} = N\gamma_\rho/f$ and the L/L_R value are the criteria defining a particular mechanism for generating front intrusions [11, 12]. In this case, L is the characteristic horizontal scale of intrusions and $L_R = N\delta H/f$ is local baroclinic Rossby deformation radius based on intrusion layer thickness δH. At $f \approx$ const and low spatial and temporal variability of the N background values in the ASF study area in the Cooperation Sea, ε is totally dependent on γ_ρ like in the subarctic frontal zone of the Pacific Ocean [11].

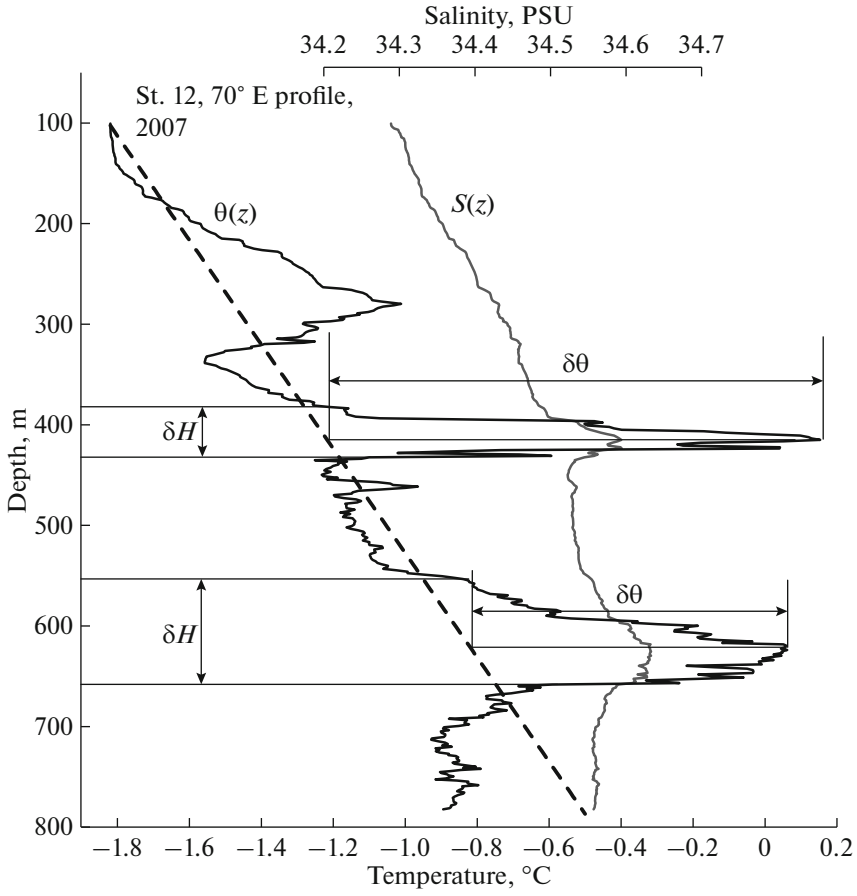

Fig. 2. Example of identification of thermohaline frontal intrusions in profiles of potential temperature $\theta(z)$ and salinity $S(z)$ at station 12 (70° E profile, 2007), which is within ASF region at top of continental slope. Dashed line is temperature background profile, δH is intrusion thickness, $\delta\theta$ is temperature anomaly in intrusion, which characterizes intrusive layering intensity in local ASF area.

Average values of ASF horizontal parameters: thermoclinity $(T_L)_\rho$ and baroclinity γ_ρ, Ri_g, ε and frontal intrusion characteristics: temperature anomaly $|\delta\theta|$, thickness δH, horizontal and transfrontal adiabatic scales $L \approx L_a$, and baroclinic deformation radius L_R in the 100–300 m upper layer and 300–600 m lower layer in Cooperation Sea in summer

Layer, m	δH, m	$\lvert\delta\theta\rvert$, °C	$\gamma_\rho \times 10^{-3}$	Ri_g	$(T_L)_\rho \times 10^{-5}$, °C/m	L_a, km	L_R, km	L_a/L_R	$\varepsilon \equiv Ri_g^{-0.5}$
100–300	83	0.44	11.3	45	5.8	10.4	1.5	6.8	0.15
300–600	67	0.45	19.7	23	18.7	2.7	1.4	1.9	0.21

For $L/L_R < 1$ in the whole range of ε values typical of the ocean, the front instability and subsequent process of intrusive layering are dependent on the thermohaline factor, i.e., double diffusion processes [11, 12]. In this case, there is always a variability area ε characterized by a decrease in intensity of intrusive layering caused by double diffusion with growth in the front baroclinity ε (i.e., with an increase in γ_ρ). When $L/L_R > 1$ and $\varepsilon > 0.01$, the baroclinic instability makes a major contribution to the instability of the thermoclinic–baroclinic front and the subsequent process of intrusive layering. For $L/L_R \sim 1$, intrusive layering depends on both factors: double diffusion and baroclinic instability [11].

The major issue in defining the intrusive layering mechanism in the ocean frontal zone is reliable determination of the intrusion transfrontal scale L using field measurement data. The high spatial interval of most measurements in the transfrontal profiles [6, 8, 11, 16, 17] prevents direct calculation of L. Therefore, taking into account the quasipycnic distribution of intrusions, the horizontal scale of each identified intrusion along the isopycnic surface was reliably estimated [16] with the help of $L_a = \delta\theta/(T_L)_\rho$, the transfrontal adiabatic scale [6]. This scale is the distance at which a water particle is transferred along the isopycnal in the presence of an isopycnic gradient of potential temperature $(T_L)_\rho$ to cause the appearance of a $\delta\theta$ anomaly in the temperature profile.

The low spatial interval between the stations in the transfrontal profiles within the ASF region in the Cooperation Sea in the recent 2011–2013 observations is $X \approx 1.8$ km and, occasionally, $X \leq 1$ km [5]. Along with the rapid completion of profiles, these data make it possible to directly estimate the intrusion horizontal scale L. Meanwhile, in previous field experiments in 2004–2007, the observation interval in the ASF region usually reached $X \approx 3$–5.5 km, thus impeding direct reliable estimation of L [1, 4]. That is why parameter L_a was also used to estimate L.

ANALYSIS OF ASF PARAMETERS AND INTRUSION SCALES

In 2004–2007 and 2011–2013, over 80 intrusions were identified and analyzed at the stations within the ASF region in the 100–600 m layer based on field measurement data on the shelf and slope of the Cooperation Sea (Fig. 1a). Intrusion layers are $\delta H \approx 20$–250 m in thickness. The δH value is comparable with the thickness of intrusions identified in the SPFZ [6] and is one of the highest values in ocean baroclinic–thermoclinic fronts. According to the detailed analysis data on all transfrontal profiles [4], the 100–600 m layer with the ASF can be conditionally subdivided into two layers (the upper layer is 100–300 m in thickness, and the lower layer is 300–600 m). These layers differ drastically in the front horizontal parameters and frontal intrusion scales, the average values of which are given in the table.

The upper 100–300 m layer is largely characterized by warm and elongated (up to 10 km and over) quasi-isopycnic intrusions (Figs. 1b, 1c) with an abundance of relatively warm MCDW at the shelf. The spatial resolution of field observations makes it possible to estimate quite reliably (up to an order of magnitude of X) the intrusion horizontal scale L in the 100–300 m layer, when intrusions are identified at a few stations in the profile (Fig. 1b; Fig. 2 in [4]). In contrast to the upper layer, the number of identified warm and cold intrusions in the 300–600 m lower layer is almost the same. On average, an intrusion thickness of $\delta H = 67$ m in the lower layer is less than in the upper layer with $\delta H = 83$ m. However, the average intensities of intrusive layering in these layers expressed in absolute temperature anomalies in the intrusions $|\delta\theta|$ are similar (~ 0.44–0.45°C) (table). Meanwhile, $|\delta\theta|$ can significantly exceed 1°C in some intrusions (Fig. 2).

A major feature of the ASF is the high degrees of baroclinity γ_ρ and thermoclinity $(T_L)_\rho$ with respect to other thermoclinic–baroclinic fronts in the World Ocean [6, 8, 11, 15, 16]. As follows from the comparison with the mesoscale horizontal parameters of the SPFZ [6], γ_ρ is three times higher, $(T_L)_\rho$ is over four times higher, and intrusive layering intensity $|\delta\theta|$ is almost twice as high in the ASF relative to SPFZ (table).

The eddy-resolving scale of field observations (especially in 2011–2013) [5] makes it possible to determine both the mesoscale and local horizontal parameters of the ASF. It turns out that their difference in the lower and upper layers is much more significant than the scales of frontal intrusions. For example, the degree of front baroclinity dependent on such parameters as γ_ρ and Ri_g is almost twice as high, and the degree of front thermoclinity $(T_L)_\rho$ is almost three times higher in the lower layer than in the upper

layer (table). Therefore, the transfrontal adiabatic scale in the lower layer $L_a \approx 2.7$ km is four times lower than in the upper layer, where $L_a \approx 10.4$ km (table). L_a in the 100–300 m layer occasionally exceeds 15 km (Fig. 2 in [4]). The L_a values obtained for the upper layer are reliable, because they are in good compliance with direct estimates of L obtained just for profile analysis (Fig. 1b).

According to the obtained estimate data, intrusion scales δH and L_a in the upper layer are much higher than those in the lower layer, but intrusion layering intensities $|\delta\theta|$ in these layers are similar (table). Why is this? As follows from correlation analysis, the lower ASF layer is characterized by a considerable positive relation between γ_ρ and $(T_L)_\rho$; in particular, a local increase in the ASF thermoclinity is accompanied by an increase in the degree of baroclinity. Therefore, the intrusion vertical scale δH decreases and horizontal scale L_a is dramatically reduced in the lower layer with respect to the upper layer (table). High intensity of intrusive layering $|\delta\theta|$ (Fig. 2) in the ASF lower layer is ensured by the high degree of front thermoclinity in local areas (Fig. 1 in [5]); these data are confirmed by the considerable positive correlation between $(T_L)_\rho$ and $|\delta\theta|$. These conclusions are consistent with those made in [16]. The higher the degree of $(T_L)_\rho$ of the front, the greater the frontal intrusion intensity, while an increase in γ_ρ of the front results in lower intrusion vertical scales δH. As for the ASF, these conclusions can be completed with the following data: a higher γ_ρ also results in a dramatic decrease in the intrusion horizontal scales L, which are reliably calculated by the field measurement data, especially those obtained in 2011–2013 [5].

Most intrusions identified in the ASF region are characterized by $L_a > L_R = N\delta H/f$ —the local baroclinic Rossby radius of deformation—on the overall background of exceptionally high degree of front baroclinity, when $\varepsilon \gg 0.01$ (table). According to [6, 11, 12], the physical nature of ASF intrusive layering and intrusion development in the front region (in both layers) is controlled by the baroclinic rather than the thermohaline factor. In the upper layer, intrusive layering is mainly due to mesoscale structure-forming processes, such as ASW flow on the sloping bottom, which forms the baroclinity density field and initiates isopycnic compensatory upwelling of warmer CDW on the shelf edge (Fig. 1b). The δH and L_a scales of CDW intrusions on the shelf edge and MCDW offshore in the upper layer significantly exceed the scales of the lower layer intrusions (table). This is because intrusive layering in the lower layer is related to local baroclinic instability of the ASF with a lower characteristic horizontal scale [5].

Then it is important to note the consistency of the average baroclinic Rossby radius of deformation of frontal intrusions $L_R = N\delta H/f \approx 1.4$ km in the lower layer (table) and the average local baroclinic Rossby radius of deformation $Rd_L \approx (g'H_{sw})^{0.5}/f \approx 1.4$ km (Table 2 in [4]) based on thickness of flowing shelf waters H_{sw} and horizontal density difference near the shelf edge $\Delta\rho_x$. In this case, $g' = (\Delta\rho_x/\rho)g$ is reduced gravitational acceleration. Rd_L and L_R were obtained independently. Similar values of the average Rd_L and L_R are indicative that the local horizontal instability scale of the front of flowing cold ASW at the shelf edge [5] is consistent with the horizontal scale of intrusive layering in the ASF region. This confirms the suggestion that the observed periodic local peaking and instability of the ASF and subsequent intensification of intrusive layering at the shelf edge are related to the event nature of the ASW flow [3, 4].

According to the estimate data on L_a and L_R, the average $L_a/L_R = 6.8$ is high in the upper layer and three times higher than $L_a/L_R = 1.9$ in the lower layer, although the average L_R values are similar in both cases. A dramatic decrease in L_a/L_R in the lower layer is also caused by a significant increase in γ_ρ and $(T_L)_\rho$ during local peaking of the ASF, resulting in drastic drop in the intrusion scales (especially L_a) (table). There is an inverse relationship between L_a/L_R and γ_ρ, as well as in the frontal zone of the Gulf Stream [8].

As follows from the conducted analysis, the initial conditional subdivision of the whole layer with intrusions in the ASF region into two layers appeared to be natural. Well-defined difference in the intrusive layering scales in these layers is due to the predominance of different intrusion generation mechanisms.

CLASSIFICATION OF FRONTAL INTRUSIONS

The analysis of numerous finely structured vertical thermohaline and density profiles at the stations falling within the ASF region in different parts of the Cooperation Sea and Prydz Bay made it possible to classify the frontal intrusions. They can be subdivided by degree of development: nonstationary intrusions in the period of front instability and intrusive layering, nonstationary vortex intrusions in the development period, and developed, so-called quasistationary, vortex intrusions. Figure 3 shows the characteristic θ and S curves for all types of cold and warm intrusions constructed from smoothed vertical thermohaline profiles (sliding average over five values) in the field of relative potential density reduced to the average depth of intrusion generation and development (σ_{400} with respect to the reference pressure level $p = 400$ db).

Some nonstationary cold intrusions and all nonstationary vortex intrusions are characterized by local density inversions in the σ_{400} profiles, which look like loops in the θ and S curves (Figs. 3a, 3c). Such density inversions indicate possible hydrostatic instability and are always supported by appropriate θ and S vertical profiles, which, even smoothed by sliding averaging,

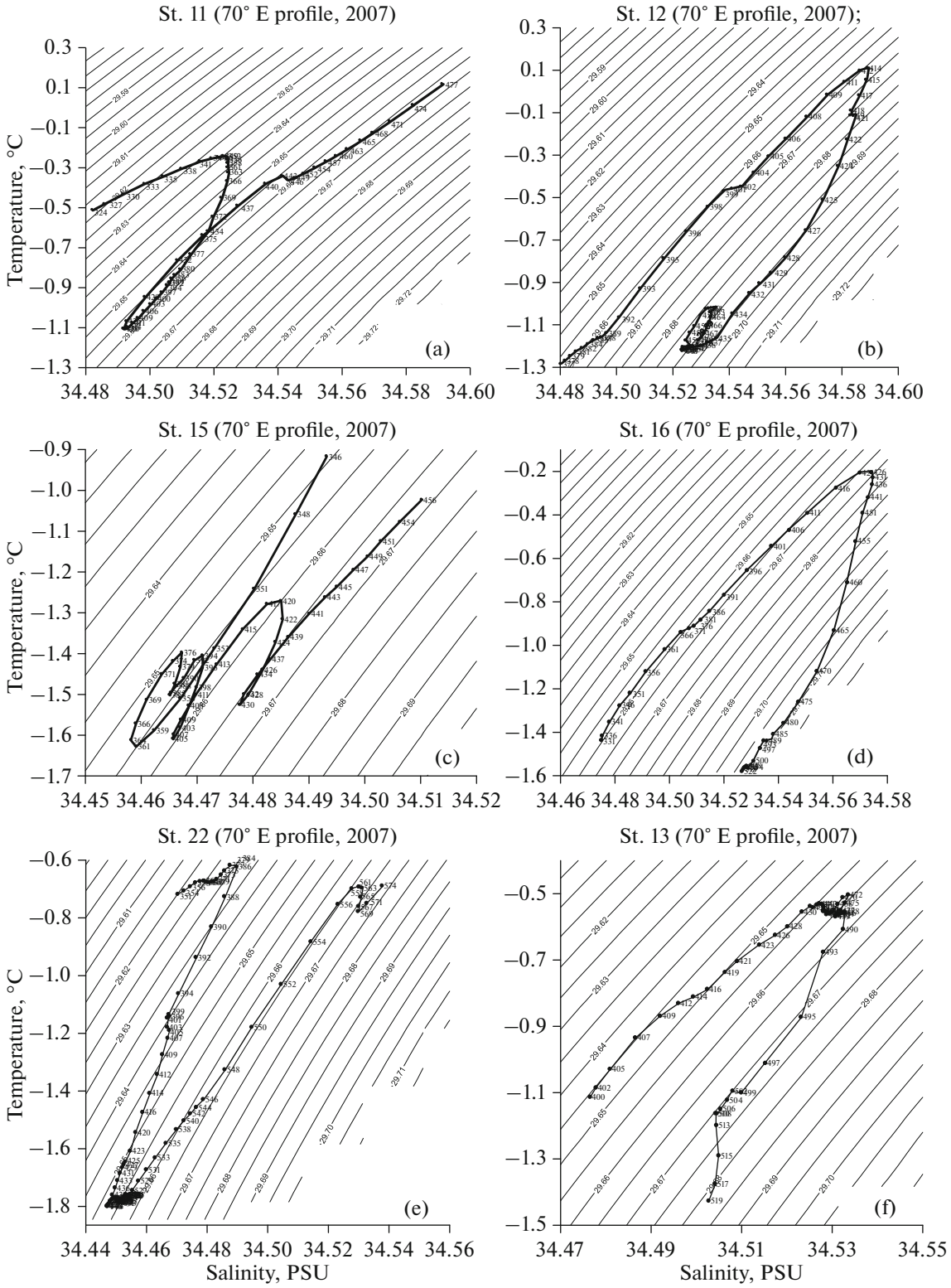

Fig. 3. Characteristic local θ and *S* curves of (a, c, e) cold and (b, d, f) warm frontal intrusions in field of relative potential density $\sigma_{400}(z)$ (smoothed by sliding average over five values) in ASF region. Nonstationary intrusions in period of the baroclinic instability: (a) cold and (b) warm, developing vortex dipole (see also Fig. 5c). Nonstationary vortex intrusions under development: (c) cold and (d) warm, vortex dipole (see also Fig. 5d). Quasistationary developed vortex intrusions: (e) cold and (f) warm (see also figs. in [3, 5]).

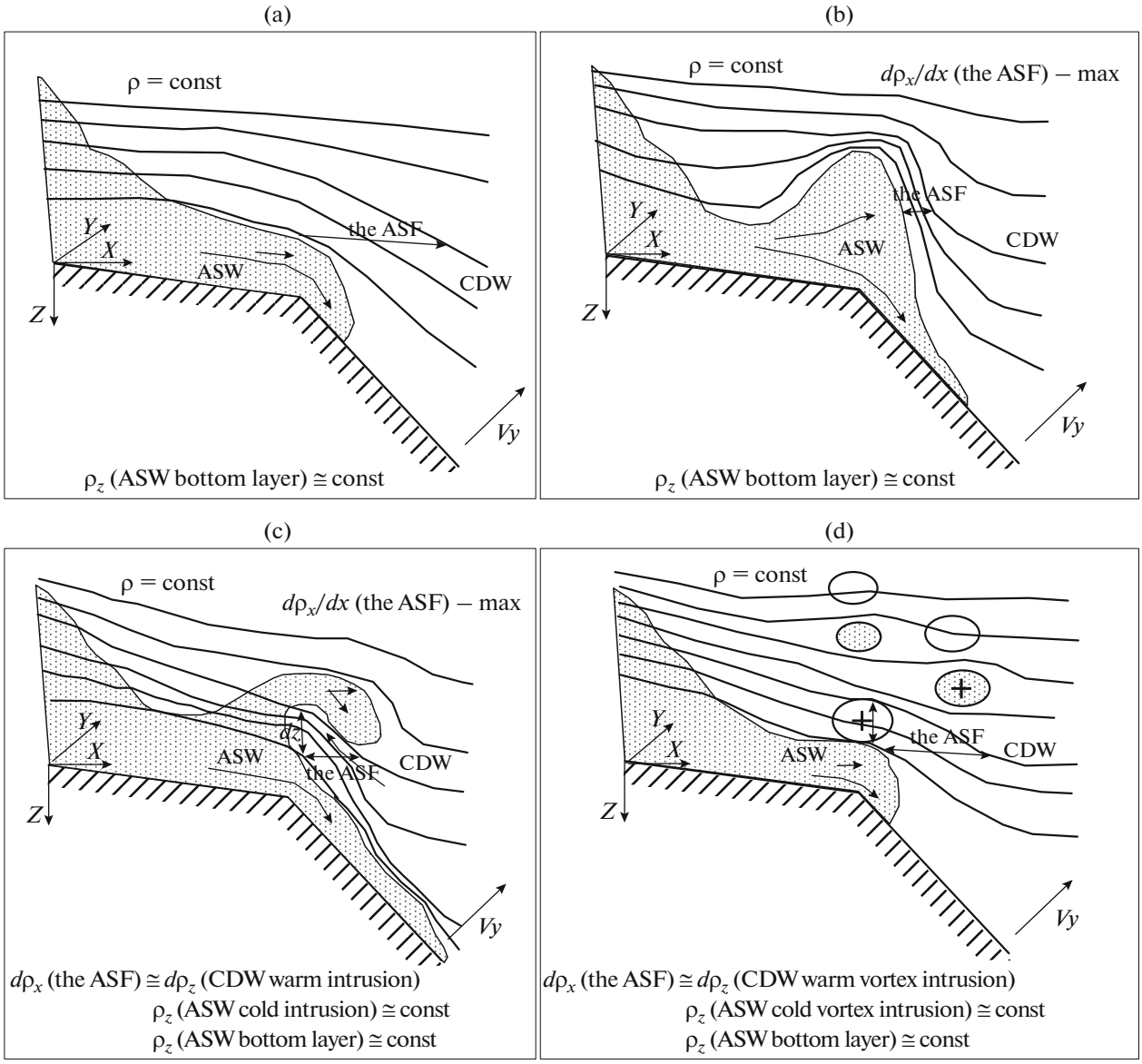

Fig. 4. ASF local baroclinic instability, four stages of development confirmed by field observation data (Fig. 5): (a) first stage, arrival of cold and dense ASW front to shelf edge; (b) second stage, ASF local peaking and thickening; highest ASF baroclinity γ_ρ and thermoclinity $(T_L)_\rho$; (c) third stage, baroclinic instability proper and intrusive layering; highest local γ_ρ and $(T_L)_\rho$ of ASF; vertical density stratification $d\rho_z$ of warm nonstationary intrusion characterizes local horizontal stratification $d\rho_x$ of ASF; vertical quasihomogeneity $\rho_z \approx$ const of cold nonstationary intrusion; (d) fourth stage, formation and development of nonstationary vortex intrusions; $d\rho_z$ (warm vortex intrusion) $\approx d\rho_x$ (ASF); ρ_z = const (cold vortex intrusion).

are distinguished by an evident irregularity (Fig. 4 in [4]; Fig. 3 in [5]). σ_{400} inversions are observed only in the ASF region. It should be noted that we analyzed only substantial σ_{400} inversions with a thickness of ~10–40 m or those "yielded" by a large number of measurements. In addition, the possibility of hydrostatic instability in the considered local intrusion layers is also confirmed by accurate calculation of the stability value: $E = (d\rho/dz)_{\text{in situ}} - (d\rho/dz)_A < 0$. In this case, $(d\rho/dz)_{\text{in situ}}$ is the vertical gradient of factual density in situ, while $(d\rho/dz)_A = g\rho/c^2$ is the adiabatic density gradient, and c is the sound velocity in a layer [4].

Inversions in the σ_{400} profiles ("pools" in the θ and S curves) likely appear due to turbulent mixing under intrusive layering after baroclinic instability in the ASF local region (Fig. 3a). Mixing of waters with different θ and S indices can result in the compaction effect characteristic of the Antarctic slope [18]. Developing and acquiring vorticity in the course of geostrophic adaptation, intrusions turn into baro-

clinic vortex intrusions [5]. This period is marked by turbulent mixing in their cores due to vorticity, which is also expressed in the density field as σ_{400} inversions (Fig. 3c).

Nonstationary warm intrusions and/or vortex intrusions also have specific local σ_{400} inversions, but only at the intrusion boundaries (Figs. 3b, 3d). They identify the turbulent mixing when water interacts with different thermohaline and density characteristics, which (as noted above) leads to the compaction effect on mixing of these waters. However, turbulence is not characteristic of cores of warm intrusions, because they are stratified by density, preventing the mixing process (Figs. 3b, 3d).

In contrast to nonstationary intrusions, developed vortex intrusions are characterized by a homogeneous or slightly stratified core (Figs. 3e, 3f; Fig. 5b in [3]). σ_{400} inversions (pools in the local θ and S curves) are not observed, which does not rule out turbulent mixing, but it does not appear in the density field, because the cores of the developed vortex intrusions are highly mixed.

SPECIFIC FEATURES OF ASF INTRUSIVE LAYERING

The ASF area can be densely packed by cold and warm intrusions and/or vortex intrusions at different stages of development, which interact with each other under equal density according to field observation data (Figs. 4d, 5c, 5d, 6a). Nonstationary intrusions and vortex intrusions (Figs. 3a–3d) are commonly observed against the background of a significant increase (by two or three times) in such ASF horizontal parameters as γ_ρ and $(T_L)_\rho$ (table; Figs. 5c, 5d), i.e., with a significant decrease in the Richardson geostrophic number $\mathrm{Ri}_g = (f/N\gamma_\rho)^2$ (table). For low variations in the background stratification in the case of local ASF peaking, Ri_g can decrease up to critical values under turbulence [8]. Reliable values of $\mathrm{Ri}_g \le 1/4$ obtained for some intrusions (Fig. 2 in [5]) are indicative of turbulent mixing due to ASF intrusive layering as water interacts with different thermohaline and density characteristics.

Direct estimations of L in the 300–600 m lower ASF layer based on field observations carried out with the vortex-resolving spatial interval (in 2011–2013) confirm that nonstationary intrusions and/or vortex intrusions are characterized by $L \approx L_R$, i.e., $L/L_R \approx 1$. As follows from analysis of the ASF stability at the shelf edge and on the slope top, the front part (or the whole front) is unstable if it is characterized by local peaking of the horizontal density gradient. In this case, diameter D of nonstationary vortex intrusions that form due to local ASF instability will be similar to the local baroclinic deformation radius of the front ($D \approx Rd_L$) [5]. Since $Rd_L \approx L_R$ (as shown above), $Rd_L \approx L_R \approx D \approx L$, as is observed in reality (Figs. 5c, 5d; Figs. 1, 2 in [5]).

The coincidence of $L \approx L_R \approx Rd_L \approx D$ values obtained by independent methods based on the field observation data is consistent with the generalized conclusions of laboratory studies of the stability of baroclinic vortices and fronts in a rotating liquid [7]. Based on this, we can assume the 3D nature of movements in the local unstable region of the ASF. The initial horizontal longitudinal frontal scale of the ASF instability Rd_L is similar in value to the horizontal transfrontal scale of intrusive layering L. Along with that, the characteristic vertical scale of the formed nonstationary intrusions δH is similar in value to the characteristic vertical scale of the ASF instability H^* [5]. In other words, L probably characterizes the local displacement scale of the ASF in the transfrontal direction during 3D baroclinic instability (Fig. 5c), which is similar to the description of the baroclinic flow instability given in [14].

However, $L/L_R \approx 1$ does not mean that thermohaline and baroclinic factors equally cause = ASF intrusive layering [10, 11], because it is a case of a very high front baroclinity $\varepsilon \gg 0.01$ (table). It can be assumed that the ASF instability and intrusive layering are caused by the baroclinic factor. Numerous signs of turbulent mixing (Fig. 3) are also indicative of this assumption. Another confirmation of the predominance of local baroclinic instability in the ASF region can be seen in Fig. 6a, where in the transfrontal profile plane in the temperature field there is a well-defined characteristic intrusive structure of the ASF. ASF local peaking (vertical) is also clearly visible (Figs. 6a, 6d). The local intrusive structure of the ASF is consistent in form with the density intrusive structure of the baroclinic front that forms during the 3D baroclinic instability studied with the theoretical model (Fig. 1c in [9]). The shape of the σ_{400} vertical profile in the ASF intrusive layering region (Fig. 6d) is also consistent with the characteristic shape of the model density deviation profile from the average state in the baroclinic front region after 3D baroclinic instability (Fig. 1d in [9]).

DEVELOPMENT OF ASF INSTABILITY

It was suggested above that intrusive layering in the lower 300–600 m ASF layer was largely due to the 3D baroclinic instability. Let us consider the instability development scheme in four stages (Fig. 4), confirmed by field observation data (Fig. 5). The first stage is the arrival of cold and dense ASW to the shelf edge as a bottom gravitational flow, which is likely to be stable in certain periods (Figs. 1b, 4a, 5a). However, as follows from analysis of the field observation data, ASW cascading is already unstable at the shelf even for low bottom slopes [4]. On the shelf edge and on the slope, a sharp increase in the bottom slope is accompanied by an increase (occasionally, by four or times) in the thickness of flowing ASW up to 150–200 m and local height peaking of the ASF, the second stage

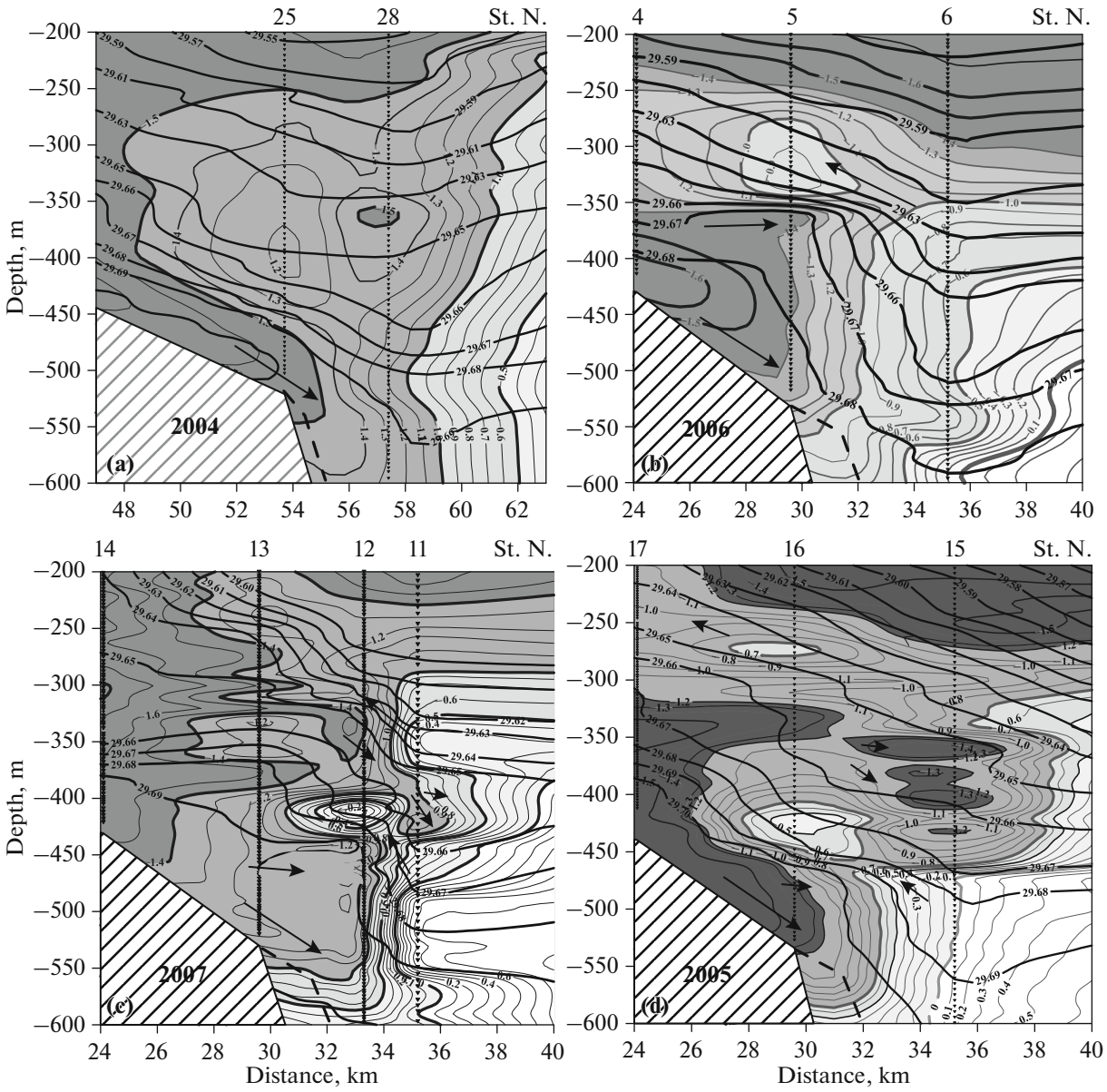

Fig. 5. Joint transfrontal profiles of 0°C and σ_{400} characterizing stages of development of ASF local baroclinic instability (Fig. 4): (a) arrival of ASW front to shelf edge (stage 1, 70° E profile, 2004); (b) ASF local peaking and thickening (stage 2, 70° E profile, 2006); (c) baroclinic instability proper and intrusion layering process (stage 3, 70° E profile, 2007); (d) formation and development of nonstationary vortex intrusions (stage 4, 70° E profile, 2005). Arrows indicate probable movements in profile plane. Specified shelf edge profile indicated by dashed line (2011–2013 observations).

(Figs. 4b, 5b). Local rise in thermoclinity (and haloclinity) $(T_L)_\rho$ results in higher the ASF baroclinity γ_ρ, when $d\rho_x/dx$ is maximum. the ASF is getting locally baroclinic [5]. At this stage, cascading becomes unstable, in particular, the ASF instability is caused by sharp increase in the bottom slope [3–5].

The next, third stage is the baroclinic instability proper: it is a short period of time, the instability moment. The baroclinic instability is induced by vertical shear of the horizontal velocity provided that this velocity shear is generated by the horizontal gradient of the potential density. In this case, the source of kinetic perturbation energy is the available baroclinic potential energy, which is rated by the local horizontal density heterogeneity [19]. At this stage, $d\rho_x/dx$ is also maximum in the ASF. The ASF instability is accompanied by front "deflection" (or "gap") and by the interpenetration of warm and cold waters, i.e., by the intrusive layering process (Figs. 4c, 5c). The front deflection is expressed as a dramatic local decrease in baroclinity up to matching of isopycnals and isobars. The front becomes almost purely thermoclinic, and

the isopycnic temperature gradient appears. This instability generates a dipole, in particular, warm and cold intrusions, which are quasi-isopycnically distributed in the transfrontal direction under equal density (Fig. 5c). Then it should be noted that the transfrontal density variation $d\rho_x$ in the ASF local region is similar to the vertical density variation $d\rho_z$ in the CDW warm nonstationary intrusion formed in the course of the ASF local instability (Figs. 4c, 5c). Meanwhile, cold intrusions are characterized by the vertical dense quasihomogeneity $\rho_z \approx$ const (Figs. 3a, 4c, 5c, 6a, 6b, 6d), which is also characteristic of the cold ASF flowing in the bottom layer at all stages of ASF instability development (Figs. 1b, 1c; Fig. 5).

The formed intrusions develop under the Coriolis force and become vortexlike. It is the fourth stage implying geostrophic adaptation, i.e., the turning of intrusions into nonstationary quasigeostrophic vortex intrusions (vortex dipoles appear). The cores of these vortex intrusions differ from adjacent waters in θ and *S* characteristics (Figs. 4d, 5d). Nonstationarity of the cold vortex intrusion is characterized by turbulent mixing in the vortex core, which is observed as inversions in the density field (Fig. 3c; Fig. 4d in [3]). Vortices are distributed quasipycnically in the ASF region (in the transfrontal profile plane), but the major movement develops towards the middle flow. This stage is also characterized by $d\rho_x$ (ASF) $\approx d\rho_z$ (CDW warm vortex intrusion) and $\rho_z \approx$ const (ASW cold vortex intrusion) (Fig. 4d, 5d). Further on, the developed baroclinic vortex intrusions are washed out in the course of viscous relaxation or are broken down into smaller vortices due to the secondary baroclinic instability (Fig. 2 in [5]).

Hence, vertical density layering of nonstationary warm intrusions characterizes horizontal stratification in the ASF local area during baroclinic instability. While the local vertical scale of the front instability $H^* \approx 30$–60 m defines the vertical scale δH of nonstationary intrusions and/or vortex intrusions (Figs. 5c, 5d; Fig. 2 in [5]).

CONCLUSIONS

The baroclinic–thermoclinic ASF forms due to the flow of dense and cold ASW. ASW cascading initiates compensatory isopycnic upwelling of warm CDW and activates slope circulation even in summer. Together they are mesoscale structure-forming processes, which form the water intrusion structure at the shelf edge and offshore. These processes under ASF local peaking are occasionally accompanied by baroclinic instability development, resulting in the formation of a smaller-scale regular intrusion structure.

Due to different processes and variable scales of intrusion layering, the ASF is naturally subdivided into two layers: the 100–300 m upper and 300–600 m lower layer. The upper layer is dominated by mesoscale compensatory isopycnic upwelling, while the bottom lower is dominated by local baroclinic instability. The front parameters and intrusion scales are very different in these layers. In the lower layer relative to the upper layer, thermoclinity $(T_L)_\rho$ is three times higher, while baroclinity γ_ρ is almost twice as high. Increase in $(T_L)_\rho$ and γ_ρ leads to decrease in the intrusion layering scales such as vertical δH and especially horizontal L_a (in four times) in the lower layer. Nevertheless, the observed intrusion intensity $|\delta\theta|$ in the lower layer is high and is provided by the elevated the ASF thermoclinity. In other words, the observation data reveal the following regularity: the higher $(T_L)_\rho$ of the front, the more intense the observed frontal intrusions, while increase in γ_ρ of the front results in the decrease of intrusion vertical and horizontal scales.

The ASF is characterized by high γ_ρ and $(T_L)_\rho$ values with respect to other thermoclinic–baroclinic fronts in the World Ocean. For example, γ_ρ is three times higher, $(T_L)_\rho$ is over four times higher, and intrusion layering intensity and temperature anomaly amplitude $|\delta\theta|$ are twice as high in the ASF than in SPFZ.

As follows from analysis of the intrusion scales and ASF horizontal parameters, the physical nature of ASF intrusive stratification is mesoscale, and the local dynamics of intrusions in the front area (in both layers) is controlled by the baroclinic factor.

Frontal intrusions can be classified by the degree of development: nonstationary intrusions in the period of ASF local instability, nonstationary vortex intrusions in the development period, and developed quasistationary vortex intrusions.

All warm intrusions in the ASF region (both layers), regardless of the formation mechanism and stage of development, are characterized by vertical stratification (but the warm and saline cores of such intrusions spread in a quasi-isopycnic way), while cold intrusions are characterized by vertical dense uniformity in the core.

The horizontal density variation in the ASF local region under baroclinic instability is similar in value to local vertical density variation in the stratified nonstationary warm intrusion that forms during the instability process.

Fig. 6. Joint transfrontal profile of θ°C and σ_{400} (69° E, 2012) characterizing (a) intrusion layering process in ASF region. Characteristic local θ and *S* curves of (b) cold and (c) warm intrusions in field of relative potential density $\sigma_{400}(z)$ (smoothed by sliding averaging over five values) and (*d*) characteristic vertical profiles of $\theta(z)$, $S(z)$, and $\sigma_{400}(z)$ (smoothed by sliding averaging over five values, index 5) at stations 25 and 26 (69° E profile, 2012) in ASF region.

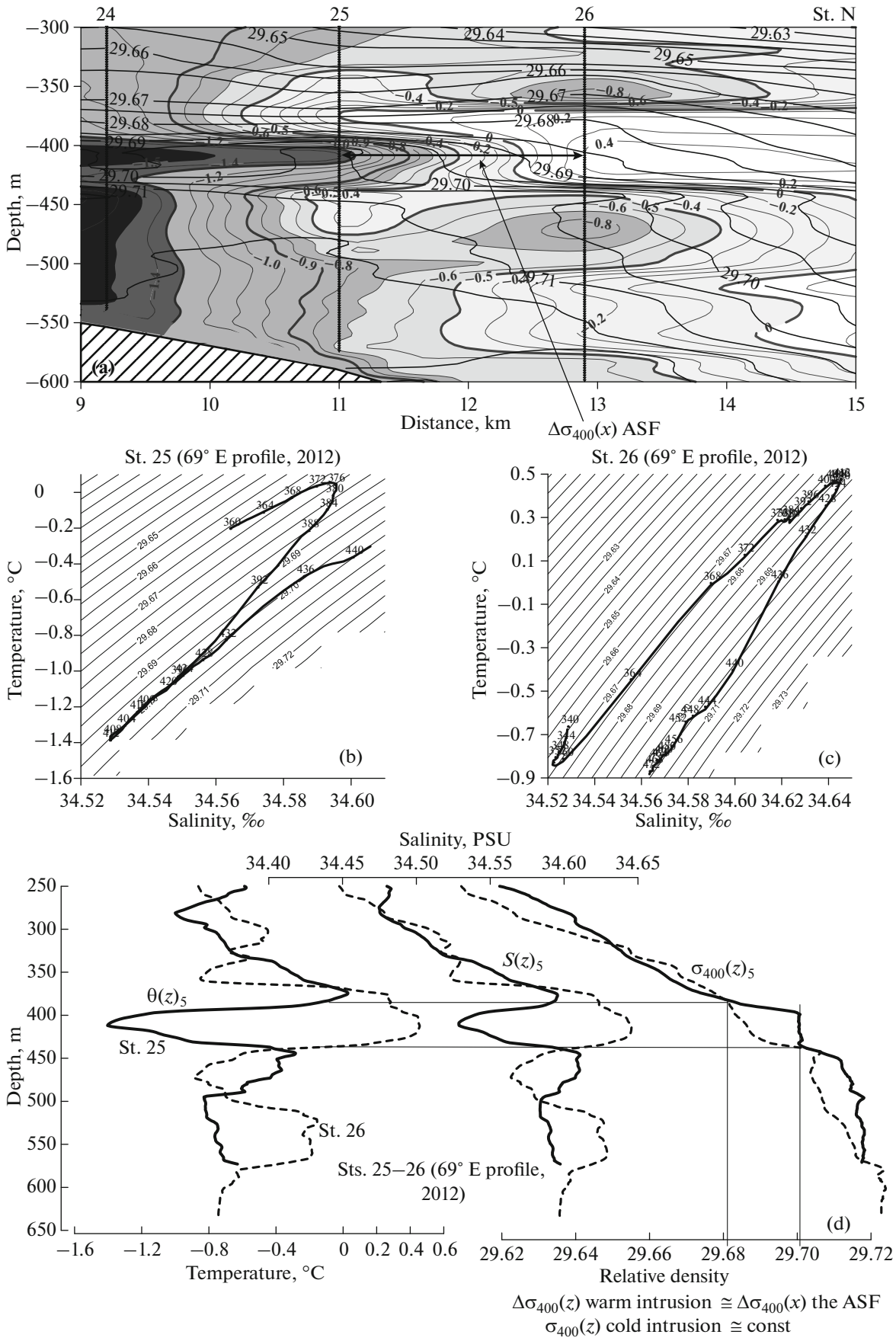
St. N
Depth, m
Distance, km
$\Delta\sigma_{400}(x)$ ASF
(a)
St. 25 (69° E profile, 2012)
St. 26 (69° E profile, 2012)
Temperature, °C
Salinity, ‰
(b)
(c)
Salinity, PSU
$\theta(z)_5$
$S(z)_5$
$\sigma_{400}(z)_5$
St. 25
St. 26
Sts. 25–26 (69° E profile, 2012)
Relative density
(d)
$\Delta\sigma_{400}(z)$ warm intrusion $\cong \Delta\sigma_{400}(x)$ the ASF
$\sigma_{400}(z)$ cold intrusion $\cong$ const

The ASF local instability is marked by a decrease in the Richardson geostrophic number Ri_g up to critical values, when turbulence is probable.

According to independent estimates, for ASF instability, the local baroclinic deformation radius Rd_L of the front is similar in value to the baroclinic deformation radius L_R of frontal intrusions based on the characteristic vertical scale of formed nonstationary intrusions δH, which in turn is similar in value to the characteristic vertical scale of the ASF instability H^* [5].

ASF baroclinic instability development can be subdivided into four stages, confirmed by field observation data. The first stage involves the arrival of ASW to the shelf edge and ASF formation. The second stage is a local increase in ASF thickness and baroclinity, ASF peaking. The third stage is baroclinic instability proper and ASF intrusive layering. The fourth stage is generation and development of nonstationary vortex intrusions (table).

REFERENCES

1. N. N. Antipov and A. V. Klepikov, "Specific oceanographic regime of the Prydz Bay according to the expedition data of the Arctic and Antarctic Research Institute in 1997–2007," Probl. Arkt. Antarkt. No. **2**, 36–48 (2007).
2. N. N. Antipov and A. V. Klepikov, "Interaction of waters of shelf and deep ocean under Antarctic continental slope," in *An Input of Russia into International Polar Year 2007/08: Oceanography and Marine Ice* (Paulsen, Moscow, 2011), pp. 291–305.
3. P. N. Golovin, "Conditions of the formation and runoff of shelf waters in different water areas of the Arctic and Antarctic," Russ. Meteorol. Hydrol. **37** (11–12), 752–761 (2012).
4. P. N. Golovin, N. N. Antipov, and A. V. Klepikov, "Downflow of the Antarctic shelf water at the shelf and continental slope of the Commonwealth Sea in the summer season and its effect on the bottom water formation in the Southern Ocean," Oceanology (Engl. Transl.) **51** (3), 370–384 (2011).
5. P. N. Golovin, N. N. Antipov, and A. V. Klepikov, "Studying the stability of the Antarctic slope front in the Commonwealth Sea," Russ. Meteorol. Hydrol. **38** (11), 766–775 (2013).
6. A. G. Zatsepin and M. V. Emel'yanov, "The pattern of intrusive lamination of waters in the Antarctic polar frontal zone of the Atlantic Ocean," Meteorol. Gidrol, No. **1**, 50–55 (1995).
7. A. G. Zatsepin and A. G. Kostyanoi, "Modeling of instability of baroclinic eddies and fronts," in *Coherent Structure and Self-Organization of Ocean Currents* (Nauka, Moscow, 1992), pp. 163–177.
8. V. M. Zhurbas, N. P. Kuz'mina, and I. D. Lozovatskii, "Role of baroclinicity in intrusive stratification of an ocean," Okeanologiya (Moscow) **28** (1), 50–53 (1988).
9. N. P. Kuz'mina, "On the vertical structure of three-dimensional intrusive interleaving of the oceanic fronts with high baroclinicity and thermoclinicity," Oceanology (Engl. Transl.) **41** (3), 338–344 (2001).
10. N. P. Kuzmina, "Vertical structure of intrusions at oceanic fronts," Russ. Meteorol. Hydrol., No. 11, 37–44 (2002).
11. N. P. Kuz'mina, V. M. Zhurbas, and A. M. Sagdiev, "Dependence of intensity of fine-structure stratification from average hydrological parameters of subarctic frontal zone of the Pacific Ocean," Okeanologiya (Moscow) **34** (2), 201–205 (1994).
12. N. P. Kuz'mina and V. B. Rodionov, "Influence of baroclinicity on development of thermohaline intrusions in the frontal ocean zones," Izv. Ross. Akad. Nauk, Fiz. Atmos. Okeana **28** (10), 1077–1086 (1992).
13. A. S. Monin and R. V. Ozmidov, *Ocean Turbulence* (Gidrometeoizdat, Leningrad, 1981) [in Russian].
14. J.S. Turner, *Buoyancy Effects in Fluids* (Cambridge Univ. Press, Cambridge, UK, 1973; Mir, Moscow, 1977).
15. K. N. Fedorov, *Physical Nature and Structure of Ocean Fronts* (Gidrometeoizdat, Leningrad, 1983) [in Russian].
16. K. N. Fedorov and S. L. Meshcheryakov, "Thermoclinicity and baroclinicity of the frontal zone of the Kuroshio Current," Okeanologiya (Moscow) **29** (3), 357–363 (1989).
17. G. I. Shapiro and M. V. Emel'yanov, "Relationship of mesoscale and fine-structure characteristics of water in the Antarctic polar frontal zone," Okeanologiya (Moscow) **34** (2), 206–211 (1994).
18. P. G. Baines and S. A. Condie, "Observations and modeling of Antarctic downslope flows: a review, in Ocean, ice, and atmosphere: interactions at the Antarctic continental margin," Antarct. Res. Ser., No. 75, 29–49 (1998).
19. E. T. Eady, "Long waves and cyclone waves," Tellus **13**, 33–52 (1949).

Translated by E. Maslennikova